JOURNAL OF SPACECRAFT AND ROCKETS
Vol. 29, No. 5, September-October 1992

Design of Hypersonic Waveriders for Aeroassisted Interplanetary Trajectories

Mark J. Lewis*
University of Maryland, College Park, Maryland 20742
and
Angus D. McRonald†
Jet Propulsion Laboratory, California Institute of Technology, Pasadena, California 91109

The aerodynamic performance of a vehicle designed to execute an aerogravity-assisted maneuver, which combines a gravitational turn with a low-drag atmosphere pass, is examined. The advantage of the aerogravity-assisted maneuver, as opposed to a more traditional gravity-assist trajectory, is that, through the use of a controlled atmospheric flight, nearly any deflection angle around a gravitating body can be realized. This holds the promise of providing extremely large values of ΔV. The success of such a maneuver depends on being able to design a vehicle which can execute sustained atmospheric lifting flight at Mach numbers in the range of 50–100 with minimal drag losses, thereby implying the use of hypersonic waveriders designed for high L/D. Some simple modeling is used to demonstrate design rules for the design of such vehicles and to estimate the deterioration of their performance during the flight. Two sample aerogravity-assisted maneuvers are detailed, including a close solar approach requiring modest ΔV and a sprint mission to Pluto.

Nomenclature

a = speed of sound
$\mathcal{R}$ = waverider aspect ratio
C = aerodynamic force coefficient
D = drag, N
G = gravitational constant
Kn = Knudsen number
L = lift, N
ℓ = waverider overall length, m
M = Mach number
m = secondary body mass, kg
n = viscosity power law coefficient
q = dynamic pressure, atm
R = body radius, m
r = orbital radius, km
t = time variable, s
V = velocity magnitude
$\bar{V}$ = normalized velocity
w = waverider base width, m
x = linear dimension
ΔV = change in velocity magnitude, km/s
δ = orbital angular deflection, rad
Θ = angle of arc through atmosphere, rad
λ = molecular mean free path, m
μ = viscosity
ν = gravitational constant times planetary mass
ρ = density, kg/m^3
Φ = total deflection angle of arc, rad
ϕ = planform half angle, rad
$\bar{\chi}$ = viscous interaction parameter

Subscripts

c = circular orbit value
e = property above boundary layer
ℓ = referenced to vehicle length
LE = leading edge
o = reference value
p = value at periapsis
w = wall value
x = streamwise value
1 = initial or approach
2 = final or exit
∞ = value at infinite distance or freestream

Introduction

AEROGRAVITY-ASSISTED interplanetary trajectories are an application of hypersonic aerodynamics to orbital maneuvering in which aerodynamic lifting forces are used to modify a vehicle's trajectory. An aerogravity-assisted flight is similar to aerobraking,[1] although, whereas aerobraking uses aerodynamic drag forces to decelerate a vehicle, an aerogravity-assisted flight would use lifting forces to redirect velocity with a minimum of energy loss.[2] Aerobraking would use high-drag hypersonic configurations to reduce orbital velocity in the atmosphere, but aerogravity-assisted vehicles must be designed to provide minimum drag for a given desired lift.

The concept of using lifting forces for control during the atmospheric flight portion of spacecraft trajectories is not new. Re-entry maneuvers typically use lifting forces to control the trajectory,[3] as will some proposed aerobraking concepts. For instance, the Apollo command module, with an $L/D \simeq 0.4$, used lifting force to augment gravity in its high-speed entry from the moon. However, the dominant force in these maneuvers is still drag, and the vehicle designs reflect that philosophy.

In the aerogravity-assist maneuver pictured in Fig. 1, a high L/D vehicle executes a cruising atmospheric pass through the atmosphere of a suitable planet and exits that planet's atmosphere back out to space, in order to boost or reduce its velocity en route to a final destination. In this way, the aerogravity-assisted maneuver is nearly identical to the more traditional gravity-assisted flight that has become common for interplanetary trajectories, with the exception that the atmospheric flight permits far greater angular deflections around the planet and thus substantially increased velocity increments. Randolph and McRonald[4] have explored applications of this concept for close solar approaches and trajectories to the outer planets. The more angular deflection that can be

Presented as Paper 91-0053 at the 29th Aerospace Sciences Meeting, Reno, NV, Jan. 7–10, 1991; received July 31, 1991; revision received Jan. 7, 1992; accepted for publication Jan. 8, 1992.

*Assistant Professor, Department of Aerospace Engineering. Member AIAA.
†Member Technical Staff. Member AIAA.

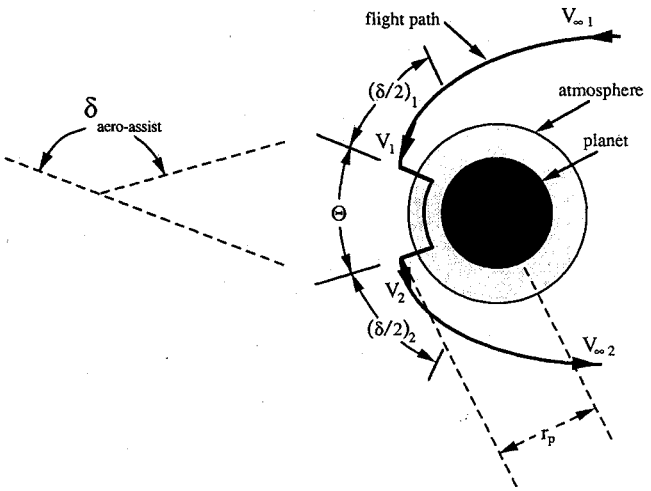

Fig. 1 Generic aerogravity-assisted maneuver, in planet-relative frame, showing angles and velocity change.

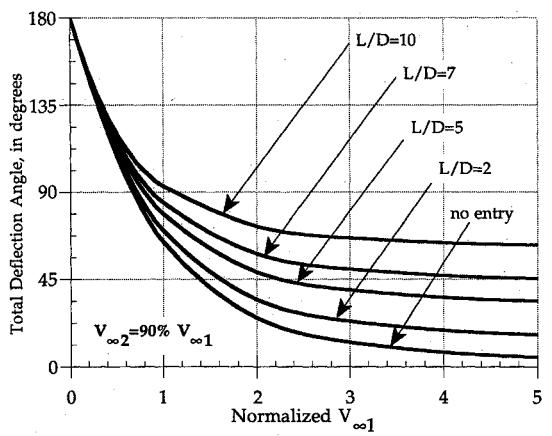

Fig. 2 Total deflection angle that can be achieved if final velocity is 90% of initial velocity, for various values of L/D.

accomplished, the greater the velocity increment in the absolute frame of reference, which is the primary advantage of the aerogravity assist.

The success of an aerogravity maneuver will depend on whether configurations which supply the required lift can be built with correspondingly small drag. If drag is prohibitively high, energy losses during the atmosphere pass will negate the advantages of the maneuver. Indeed, the analysis below will show that the configurational ratio of lift-to-drag (L/D) is the governing parameter in determining energy losses through the maneuver,[5,6] a fact which is not surprising given that the atmospheric flight is nearly constant-speed cruise.

A successful aerogravity-assisted maneuver would require a configuration with high lift-to-drag ratio, relative to traditional re-entry shapes, to minimize energy losses due to atmospheric drag while energy is being gained through the use of lift. Figure 2 demonstrates this by presenting a plot of deflection angle that can be accomplished with 10% energy loss vs the incoming velocity normalized to circular orbit velocity at periapsis, as a function of L/D. Not surprisingly, at higher L/D, there are fewer losses for a given required lift. Figure 3 provides another indication of this effect by displaying the velocity at exit from an aerogravity-assisted flight which executes a 135-deg turn, vs the normalized incoming velocity, once again as a function of L/D.

The requirement for high L/D immediately suggests the class of configurations known as "waveriders," first conceived by Nonweiler in 1959.[7] Waveriders are vehicles that are designed so that the bow shock is everywhere attached to the sharp leading edge. In this way, the vehicle is riding on a cushion of high-pressure fluid, which is contained between the bow shock and the undersurface. Because waveriders have shown both theoretical and experimental promise of providing the highest possible values of L/D, this paper will focus on that specific application.

If the aerogravity-assisted flight is to be viable, several questions must be explored in regard to waverider performance:

1) What values of realistic L/D ratios can be expected for aerogravity-assisted vehicles, and can these be sustained throughout the flight?

2) What levels of heating can be expected on such a vehicle?

3) How much acceleration will be experienced by the vehicle (of particular importance if a crew is present)?

4) What control issues must be identified, and are there reasonable hopes of controllable flight under required trajectory conditions?

5) Can the same aerodynamic configuration be used for more than one aeropass, possibly at different planets?

It will be the goal of this present work to address some of these questions, at least in application to the specific trajectories cited, and to suggest possible limits for other aerogravity-assisted flight operations.

Applicability of the Waverider for High L/D

The preceding arguments have served to emphasize that the effectiveness of these sorts of planetary maneuvers depends on the realization of high values of L/D. This will require the use of a waverider. Waveriders are a family of flight configurations that are derived by solving for a flow surface which intersects a known shock flowfield, such as that generated by a cone or power-law body. The process of designing a waverider has been described extensively in previous work.[8] The advantage of the waverider is that the shock is everywhere attached to the outer edge of the vehicle. This prevents spillage and so permits the vehicle to derive maximum lift from the shock compression.

In fact, waverider designs have been analyzed which would provide reasonable values of L/D. The work by Bowcutt et al.[9,10] and Corda and Anderson[8] resulted in a family of optimized waverider designs wherein the effects of skin-friction drag were included within the optimization process. These waveriders demonstrate the potential for higher lift-to-drag ratios and/or lower minimum drag coefficients than other hypersonic configurations examined to date.

A typical "viscous-optimized" waverider is shown in Fig. 4, which is a three-view of a waverider designed for Mach 20 operation in Earth's atmosphere. This particular waverider is 2 m long and has been optimized for both maximum L/D and high volume at 60-km altitude. Planetary waveriders have been shown to closely resemble terrestrial designs at similar Mach number and dynamic pressures.[11]

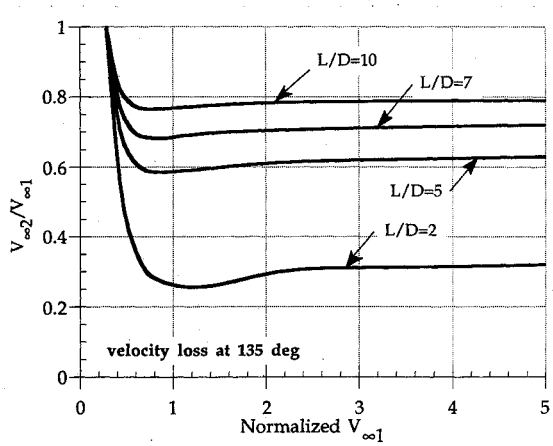

Fig. 3 Velocity at completion of an aerogravity-assisted maneuver as a function of L/D ratio, assuming 135 deg total turning angle.

Aerogravity-Assisted Trajectories

Figure 5 presents a schematic of the trajectories followed by a waverider in an aerogravity-assisted flight to either the sun or an outer planet such as Pluto. The following are two such representative trajectories.

Earth-Venus-Mars-Sun

The Earth-Venus-Mars-Sun (EVMS) aerogravity-assisted trajectory of primary interest would be suitable for the proposed Jet Propulsion Laboratory Solar Probe Mission, the goal of which is to place an instrument package within four solar radii of the sun (0.0186 AU). To accomplish this mission without benefit of an assist would require total ΔV of 24 km/s.

The EVMS mission begins on June 14, 2007, with an Earth launch and ΔV of 6.20 km/s. The vehicle reaches Venus on August 10, 2007, with an approach velocity of 17.47 km/s, enters the Cytherean atmosphere at Mach 80, and turns through 79.47 deg, of which 62.76 deg occurs in the atmosphere, which launches it on a trajectory toward Mars. Mars is reached on October 23, 2007, with an approach velocity of 24.81 km/s, leading to flight at Mach numbers in excess of 100. The vehicle turns through a total of 82.68 deg around Mars, including 80.43 deg in the atmosphere, reaching aphelion on November 16, 2007, and solar perihelion on March 20, 2008.

Without the Cytherean aeroassist, a simple gravity assist could accomplish at most 16.53 deg, assuming closest passage at 160 km altitude, the lower extent of the Cytherean exosphere. This means that an extra 62.94 deg is accomplished by flying through the atmosphere of the planet. Note that the angular deflection that has been added by the maneuver is slightly higher than the actual deflection that occurs in the atmosphere, which was just quoted. This is because the aeropass results in some loss of velocity, so the outgoing hyperbolic turn has a larger angular deflection, and because the radius of closest approach to the planet is reduced, which also increases the overall angular deflection along the hyperbolic portions of the flight.

One way to think about the aeroassisted trajectory is to treat it as a traditional nonaerodynamic gravity-assisted maneuver with a substantially reduced radius of periapsis. The trajectory under consideration would have an "effective radius" of 601 km closest approach. This means that the aeromaneuver at altitude produces the same result as a nonaeroflight at a periapsis which is 5568 km beneath the planet's surface (neglecting velocity loss due to drag). At Mars, a simple gravity assist would provide 2.20-deg deflection with 130-km altitude closest approach, so the aeroassisted maneuver adds 80.48 deg to the deflection angle. In this way, it resembles a simple gravity assist with an effective periapsis radius of 35.77 km from the center of the planet. Although this modeling has included drag losses, it is in fact possible that these losses could be offset, perhaps with exhaust from an active cooling system.

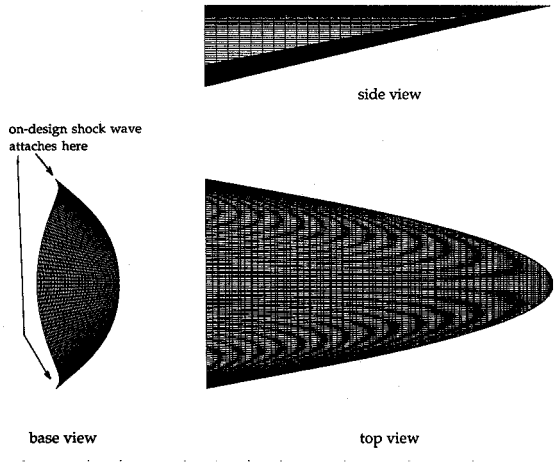

Fig. 4 Schematic of representative flights performing aerogravity assists in the atmospheres of Venus and Mars.

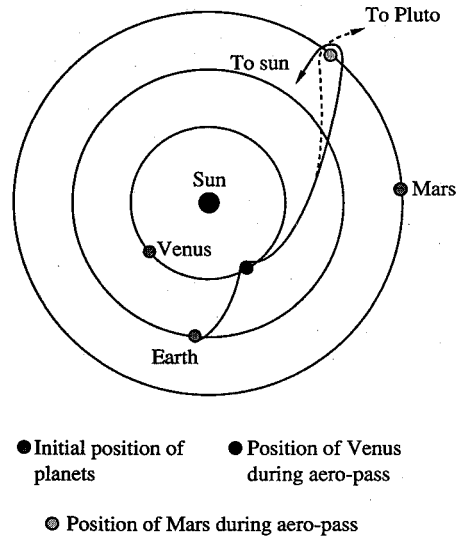

Fig. 5 Typical waverider shape, in this case a 2-m-long vehicle optimized for maximum L/D and volume, designed for flight at 60-km altitude at Mach 20 in Earth's atmosphere.

Earth-Venus-Mars-Pluto

The Earth-Venus-Mars-Pluto aerogravity-assisted trajectory has been proposed to provide a rapid flight to the outermost planet. The proposed trajectory, which would launch on October 26, 2013, reaches Pluto almost exactly 5 years later. This is in contrast to the 12-15 years that would be required for a more conventional trajectory.

Initial ΔV is 5.09 km/s, with an aphelion 2 days later, followed by an aerogravity-assisted turn at Venus on January 5, 2014, with an approach velocity of 13.85 km/s, and a turning angle of 116.05 deg, of which 91.20 deg is accomplished in the atmosphere while flying at Mach 70. This puts the vehicle on course to Mars, approaching on March 27, 2014, with velocity 24.43 km/s and a resulting 76.70-deg turn, of which 74.35 deg occurs in atmosphere, with subsequent approach to Pluto on October 26, 2018.

The atmospheric maneuver at Venus adds 91.71 deg to the 24.34 deg that could be accomplished with a traditional gravity assist. The aerogravity assist looks like a traditional gravity assist with periapsis radius of 303 km from the center of the planet. At Mars, only 2.31 deg could have been accomplished with a gravity-assisted flight; the remaining 74.38 deg is realized in the aeroassist. This would correspond to a gravity turn at 43.95 km periapsis radial distance from the planet's center.

Aeroassisted Hyperbolic Trajectory

The dynamics of an aerogravity-assisted vehicle will be reviewed briefly. A trajectory with an atmospheric passage provides unlimited capability to modify the flight direction, with the constraint that velocity magnitude is lost to drag during the course of the flight. A vehicle entering the atmosphere will experience a deceleration given by

$$dV = -(D/m)\,dt \tag{1}$$

where D/m is the drag force divided by the vehicle mass. Since it is most convenient to characterize the vehicle in terms of the lift-to-drag ratio L/D, this is written as

$$dV = -[L/(L/D)m]\,dt \tag{2}$$

The time of flight can be related to the arc length Θ traveled at radius r in the atmosphere since $V\,dt = r\,d\Theta$. If it is assumed

that approximately constant-altitude flight is to be achieved, lift must be used to add to gravitational forces in counteracting the excess centrifugal effects. This means that the waverider is flying "upside-down" with respect to the planet's surface, using its lift to augment gravity and maintain constant r:

$$L + \nu m/r^2 = mV^2/r \tag{3}$$

so that Eq. (2) can be rewritten as

$$dV = -(L/D)^{-1}[V - (\nu/rV)]\, d\Theta \tag{4}$$

This can be integrated, with the goal of expressing the velocity as a function of Θ, provided that the variation of the L/D ratio with flight velocity is known. Off-design performance of a hypersonic waverider is not well known and is in fact a current topic of research. There is a traditional suspicion that waveriders will perform poorly at off-design conditions, although the rule of hypersonic Mach-number independence suggests that, in fact, the L/D ratio should be relatively insensitive to changes in Mach number alone. Indeed, the governing geometry becomes insensitive at high Mach numbers.[12]

The dominant variation in vehicle performance will be a result of the reduced lift requirements as flight velocity is lost to drag. Consider for instance a vehicle which enters an atmosphere at a speed in excess of orbital velocity and at some assumed high value of L/D. At the point where drag reduces the velocity to orbital speed no aerodynamic lift is required, so L/D will have dropped to zero. This is of course an unusual case, as normally the vehicle would exit the atmosphere, completing its atmospheric maneuver before its velocity fell to orbital speed.

In this example, lift could be reduced by either changing angle of attack, increasing flight altitude, or both. Changes in angle of attack will result in variations in the coefficient of lift C_L and the coefficient of drag C_D and therefore the lift-to-drag ratio L/D. On the other hand, increasing flight altitude will have minimal effect on the lift and drag coefficients while changing the magnitude of lift by reducing the ambient density since lift is proportional to ρ. Increasing altitude will decrease the Reynolds number and thereby increase viscous effects such that drag coefficient is increased.

With the assumption of constant L/D, Eq. (4) can be solved directly. The vehicle will travel through an angle Θ at altitude r where

$$\Theta = -\left(\frac{L}{D}\right)\int_{V_1}^{V_2} \frac{dV}{V - \nu/rV} \tag{5}$$

$$= -\frac{1}{2}\left(\frac{L}{D}\right) \ln\left\{\frac{V_2^2 - \nu/r}{V_1^2 - \nu/r}\right\} \tag{6}$$

in which it is assumed that L/D is approximately constant or at least can be characterized by some constant value during the flight. Note that this assumption will fail as the vehicle's velocity approaches the circular orbit velocity, for under those circumstances lift goes to zero, and with fixed L/D, so does drag.

The atmospheric exit velocity can be written in terms of the atmospheric entrance velocity:

$$V_2 = \sqrt{e^{\frac{-2\Theta}{(L/D)}} V_1^2 - [(e^{\frac{-2\Theta}{(L/D)}} - 1)(\nu/r)]} \tag{7}$$

To treat the entire maneuver in "black box" manner, with an input velocity and output velocity, it is convenient to relate final velocity at infinity in terms of the initial relative approach velocity:

$$V_{\infty 2} = \sqrt{e^{\frac{-2\Theta}{(L/D)}} V_{\infty 1}^2 + [(e^{\frac{-2\Theta}{(L/D)}} - 1)(\nu/r)]} \tag{8}$$

Note that, as expected, drag in the planetary atmosphere has decreased the incoming velocity by an amount governed by the exponential scale factor $2\Theta/(L/D)$. The total turning angle Φ, including gravity-only and atmospheric components, is[5]

$$\Phi = \Theta + \sin^{-1}\left(\frac{1}{1 + rV^2/\nu}\right) + \sin^{-1}\left[\frac{e^{(2\Theta/(L/D)}1}{1 + rV^2/\nu}\right] \tag{9}$$

Aerodynamic Modeling and Performance Losses

Viscous Scaling

A viscous-optimized waverider is designed with a single goal, usually of providing maximum L/D under suitable geometric constraints; however, since waveriders are configured for a single design point (both Mach number and Reynolds number) attention must be paid to the off-design performance of the vehicle in an aeromaneuver.

It is likely that, during flight, the L/D will decrease from the optimum design value. Furthermore, it is likely that, under the extreme heating conditions characteristic of an aerogravity-assist atmospheric cruise, the waverider will be losing leading-edge material and the resulting bluntness may also decrease L/D. In this section, we will attempt to model the off-design performance of a waverider and determine some simple strategies for adjusting the generated lift so as to maximize L/D throughout the flight.

Although waveriders have associated with those flowfields that are fundamentally three dimensional, the very nature of the waverider permits some important simplifications. Streamlines on a waverider tend to be highly two dimensional, because the attached bow shock prevents secondary flow around the leading edge. Thus, it is relatively accurate to model waverider flow as moving straight back along the surface of the vehicle. The waveriders of most interest are designed from axisymmetric flowfields, such as that associated with a cone; however, experience has shown that optimization processes tend to result in shapes which reside in regions of the design flowfield with relatively small curvature. In other words, even though the waverider may be carved from a three-dimensional flowfield, it is still generally accurate to model it as a two-dimensional surface with nearly planar shocks. In this respect, waveriders have a gross resemblance to delta wings, though the promised L/D is higher. Finally, it is reasonable to assume that the requirement for a sharp leading edge will result in insignificant bluntness effects.

In hypersonic aerodynamics, a fundamental nondimensional number is the viscous interaction parameter $\bar{\chi}$, which indicates the strength of interactions between a shock wave and the boundary layer on a surface:

$$\bar{\chi} = M_\infty^3 \sqrt{C}/\sqrt{Re_{x,\infty}} \tag{10}$$

where $C = (\rho\mu)_{\text{wall}}/(\rho\mu)_{\text{inviscid}}$. At values of $\bar{\chi} > 3$, the shock above a surface interacts strongly with the boundary layer on that surface.[13] From this, a length can be derived which indicates whether strong interactions are important:

$$x_{\text{strong}} = (1/9)(M_\infty^5 C \mu_\infty/\rho a_\infty) \tag{11}$$

Assuming constant pressure normal to the surface and using a power-law approximation for viscosity, C can be written in terms of temperature only:

$$x_{\text{strong}} = (1/9)[M_\infty^5 (T_{\text{wall}}/T_{\text{inviscid}})^{n-1}(\mu_\infty/\rho a_\infty)] \tag{12}$$

With an adiabatic wall and assuming that wall temperature is approximately the total temperature, this can further be approximated as

$$x_{\text{strong}} \approx (1/9)[M_\infty^{2n+3}[(\gamma - 1)/2]^{n-1}(\mu_\infty/\rho a_\infty)] \tag{13}$$

Using Chapman's result that relates viscosity to mean free path, $\mu \simeq 0.67\rho\lambda a$, the interaction length becomes $x_{\text{strong}} =$

$0.074M_\infty^{2n+3}[(\gamma-1)/12]^{n-1}\lambda$. In air, with $\gamma = 1.4$ and $n = 0.67$, $x_{strong} = 0.126M_\infty^{4.34}\lambda$, whereas in a CO_2 atmosphere such as that of Mars or Venus, with $\gamma = 1.33$ and $n = 0.79$, $x_{strong} = 0.108M_\infty^{4.58}\lambda$.

For conditions associated with all of the portions of the Venus and Mars aeroassisted trajectories, the strong interaction length will be on the order of tens to hundreds of meters. Thus, except in cases of highly cooled walls, these planetary waveriders must be designed with strong interactions between boundary layer and shock considered. This will increase drag, decrease lift, change moments, and generally result in different optimized waverider shapes than those designed without considering strong interactions.

Lift Approximation

Using the principles just stated, flow over a waverider will be modeled here with straight streamlines over a delta-shaped flat plate at some apparent angle of incidence. If the waverider is at apparent incidence angle θ and has area A, Lee's modified Newtonian theory predicts, for small angles and high Mach numbers, lift

$$L = \tfrac{1}{2}C_{p_{max}}\rho U^2\theta^2 A \tag{14}$$

where $C_{p_{max}} = 1.84$ for terrestrial air and 1.86 for the CO_2 of the Martian and Cytherean atmospheres.

Newtonian theory is inaccurate at small angles of incidence and is best used as a basis of comparison for other more accurate solutions. Lift is better estimated with tangent wedge theory, which predicts a shock pressure ratio over an inclined surface of

$$\frac{p_e}{p_\infty} = 1 + \gamma\frac{\gamma+1}{4}M^2\theta^2 + \gamma M^2\theta^2\sqrt{\left(\frac{\gamma+1}{4}\right)^2 + \frac{1}{M^2\theta^2}} \tag{15}$$

In the limit of $M^2\theta^2 \gg 1$, $p_e/p_\infty \approx \gamma[(\gamma+1)/2]M^2\theta^2$.

For flight conditions of interest here, this pressure ratio must in turn be modified for strong interaction effects. White has developed estimates of the pressure distribution over an inclined surface with shock-boundary-layer interaction effects included, as an extension of the flat-plate strong interaction work of Bertram and Blackstock.[14] In general, flight Mach numbers for these craft, especially on interplanetary trajectories, will be in the range of 30–100, and effective deflection angles will be at most 5–10 deg. This will lead to values of $M^2\theta^2 \approx 7$–300. With $M\theta > 10$, pressure on a cold inclined surface, relative to freestream pressure, is

$$\frac{p_e}{p_\infty} \approx 1 + \frac{\gamma(\gamma+1)}{2}M^2\theta^2 + 0.15\bar{\chi}(\gamma-1)\sqrt{2\gamma(\gamma+1)} \tag{16}$$

This would represent the pressure at some position along a streamline which corresponds to a given value of $\bar{\chi}$ on the lower surface of a waverider. Note that it is the tangent wedge pressure with an added contribution due to shock-boundary-layer interaction.

The upper surface will be aligned with the freestream, or nearly so, so that the pressure distribution there comes from the result of strong interaction on a flat surface,[14] which indicates that the pressure ratio is insensitive to angle, so long as the angle is nearly zero.

$$p_e/p_\infty \approx 1 + 0.61(\gamma-1)\sqrt{\gamma(\gamma+1)}\,\bar{\chi} \tag{17}$$

This equation is strictly for insulated surfaces; for a completely cooled wall the additional pressure due to the strong interaction is roughly one-fourth the value that would be calculated with Eq. (17). Substituting for $\bar{\chi}$ from Eq. (10), and using a similar development to that for Eq. (13), and substituting for properties of CO_2, these expressions become as follows:

Lower surface:

$$p_e/p_\infty \approx 1 + 1.55M^2\theta^2 + 0.12M_\infty^{2.29}\sqrt{Kn} \tag{18}$$

Upper surface:

$$p_e/p_\infty \approx 1 + 0.40M_\infty^{2.29}\sqrt{Kn} \tag{19}$$

where Kn is Knudsen number λ/x. Integrating the upward component of the net pressure on a triangular planform of length ℓ, width w, and aspect ratio $AR = 2w/\ell$, with a lower surface at angle θ to the freestream, as shown in Fig. 6, lift is

$$L = 2p_\infty\int_0^{\ell AR/4}\int_0^{4y/AR}\Big[1.55M_\infty^2\theta^2 + (0.12\sqrt{\cos\theta} - 0.40)M_\infty^{2.29}\sqrt{\lambda/x}\Big]\,dx\,dy \tag{20}$$

$$\simeq \rho U^2[0.29\theta^2 - (0.15 + 0.02\theta^2)M_\infty^{0.29}\sqrt{Kn_\ell}]\,\ell^2\,AR \tag{21}$$

where Kn_ℓ is the Knudsen number based on overall vehicle length. Note that the effect of viscous interactions, contained in the Knudsen-number-dependent term, will reduce the lift for all practical waveriders and that this effect is a very weak function of Mach number and θ. Strong interaction effects are in fact sensitive to $M\theta$ for moderately large values of that similarity parameter, but in the case of planetary vehicles the upper surface has $M\theta$ too small and the lower surface has $M\theta$ too large for the effect to be of significance. For small Knudsen number, the lift is simply the tangent wedge solution; since the area of the triangular planform is $A = \frac{1}{4}(\ell^2 AR)$, lift will be $L = 1.17\rho U^2\theta^2 A$ in the Cytherean and Martian atmospheres, which is about 20% higher than the prediction of modified Newtonian theory.

Drag Prediction

Following the preceding arguments, waverider drag performance will be modeled by dividing the drag into three basic components: 1) wave drag, 2) skin friction, and 3) leading-edge bluntness.

To do so, the waverider will once again be assumed to have a delta planform, which ignores the fact that waveriders in fact tend to have curved leading edges and often blunted frontal regions. With length ℓ, width w, and aspect ratio $AR = 2w/\ell$, leading-edge length is $\ell[1 + AR^2/16]^{1/2}$. Strong interaction effects will tend to increase both wave drag and skin friction by making the shock waves stronger and reducing boundary-layer thickness (and thus increasing gradients). The former effect can be reduced by proper shaping of the surface and is generally of less importance than the latter phenomenon.

Wave Drag

Wave drag can be estimated from the shock-pressure ratio following the method by which lift was estimated. It has previously been seen that strong viscous interaction effects are most significant on the upper surface; since these will not contribute greatly to drag, tangent wedge theory will be used to estimate drag: $D = 1.17\rho U^2 A\theta^3$ in a CO_2 atmosphere. Sub-

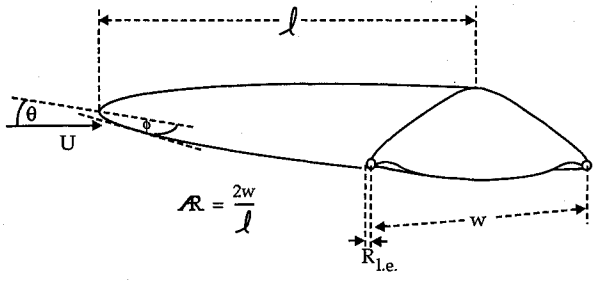

Fig. 6 Nomenclature for simple model of waverider flowfield.

stituting for planform area in terms of overall length and aspect ratio,

$$D_{\text{Newtonian}} = 0.29\rho U^2 \ell^2 \mathcal{R}\theta^3 \tag{22}$$

Once again, the angle θ is an "effective" angle of incidence to the flow, which is best defined in terms of the aerodynamic performance.

Leading-Edge Bluntness

Newtonian theory is quite accurate in predicting forces on blunted objects. Force on a cylinder with radius R_{LE} is $D_{LE} = \frac{1}{3}C_{p_{\max}}\rho U^2_{\text{normal}} R_{LE} s$, where s is the length of the cylinder and U_{normal} is the velocity normal to the cylinder. The leading edge will be modeled as resembling a half cylinder. For a CO_2 atmosphere, the two waverider leading edges will therefore experience a normal force $F_{LE} = 1.24\rho U^2_{\text{normal}} R_{LE} \ell [1 + \mathcal{R}^2/16]^{\frac{1}{2}}$.

The normal velocity, U_{normal} which appears in the drag equation, is the component of the freestream velocity perpendicular to the leading edge. If the leading edge makes an angle ϕ with the freestream, the component of force on the cylinder opposing the motion of the vehicle will be the net drag, $D_{LE} = 1.24\rho U^2 \sin\phi^3 R_{LE} \ell [1 + \mathcal{R}^2/16]^{\frac{1}{2}}$. Note that the sine of the relative angle ϕ is cubed in this equation, since it appears not only in the velocity term but also in the direction in which net drag is transmitted to the vehicle.

The leading-edge radius is most readily considered in terms of the overall length of the vehicle, so it will be more convenient to define $\bar{R}_{LE} = R_{LE}/\ell$. The angle ϕ can be defined in terms of the dimensions just defined: $\sin\phi = \mathcal{R}/[16 + \mathcal{R}]^{\frac{1}{2}}$. Thus, the leading-edge bluntness drag is

$$D_{LE} = 0.62\rho U^2 \bar{R}_{LE} \ell^2 [\mathcal{R}^3/(32 + 2\mathcal{R}^2)] \tag{23}$$

This development has assumed that all of the waverider leading-edge bluntness contributes to drag. This is true if there is neither anhedral or dihedral. In fact, waverider designs tend to exhibit anhedral, so some of the force generated on a blunt leading edge may contribute to the lift of the vehicle if the leading edge has an effective incident angle with the freestream. If the apparent anhedral angle of the leading edge goes to 90 deg downward, leading-edge bluntness makes no contribution to drag if the leading-edge incidence angle is zero relative to the flight direction. For small leading-edge incidence, bluntness produces more lift than drag, so large anhedral can be used to increase L/D with bluntness. Thus, this development is a worst-case drag model.

Several other effects of leading-edge bluntness have not been included in this analysis and require a development which is beyond the scope of this treatment. As the leading edge blunts, the pressure gradient at the leading edge will become increasingly more favorable to the surface boundary layer. Thus, the increase in drag due to bluntness may be offset by diminished viscous losses on the rest of the vehicle. Furthermore, increased bluntness may mean reduced temperatures at the leading edge, which will also reduce viscous losses there. This once again suggests that the preceding model will overpredict the effect of bluntness in increasing drag. A negative aspect of leading-edge bluntness that has not been included will be that the bow-shock detachment distance will increase, thereby permitting flow leakage from the lower surface and reducing the flowfield containment effect of the waverider shape.

Table 1 Maximum L/D and corresponding θ for Venus aero-assist waveriders

Waverider length ℓ	$\theta_{\max.\,L/D}$, deg	$L/D_{\max.}$
1	10.2	2.8
10	5.8	5.0
50	4.0	7.3
100	3.3	8.7

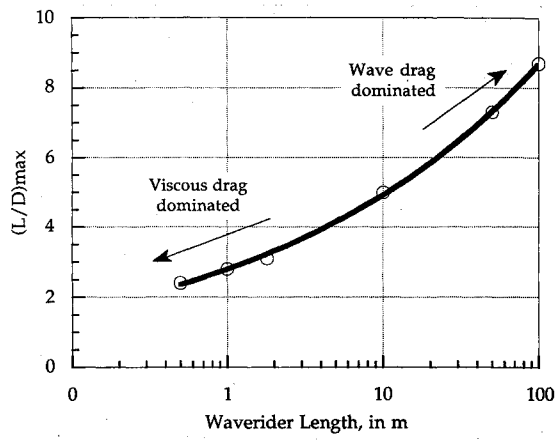

Fig. 7 Variation in maximum L/D with vehicle length, for flight at 80 km in the Cytherean atmosphere. Note that for long vehicles, wave drag dominates and high values of L/D are realizable; for smaller vehicles, Reynolds numbers are also smaller for a given altitude, and this viscous drag dominates the performance.

Viscous Surface Drag

The very high Mach numbers associated with aeroassisted flight suggest that boundary layers will be entirely laminar over all but the largest of waverider bodies. Once again, the waverider permits the assumption that streamlines run straight back along the vehicle surface, so that the drag may be estimated by integrating over the entire vehicle area as a series of two-dimensional streamlines.

Reynolds analogy can be modified for a hypersonic flat plate, and the result is that the skin friction is given by

$$C_f \approx 0.664\sqrt{\frac{p_e}{p_\infty}\frac{C}{Re_{x\infty}}} \tag{24}$$

where p_e/p_∞ is the ratio of inviscid shock-layer pressure to the freestream pressure, and C is the Chapman-Rubesin parameter already defined. White[13] has integrated along a surface of length ℓ, with a pressure distribution that is linear with $\bar{\chi}$, such that

$$p_e/p_\infty = P_o + (k/\sqrt{\bar{x}}) \tag{25}$$

the coefficient of drag along a streamline of length ℓ is

$$C_D = 1.328\sqrt{\frac{P_o C}{Re_{\ell\infty}}}\left(\sqrt{1 + \frac{k}{P_o\sqrt{\ell}}} + \frac{k}{2P_o\sqrt{\ell}}\ln \times \left[\frac{\sqrt{1 + (k/P_o\sqrt{\ell})} + 1}{\sqrt{1 + (k/P_o\sqrt{\ell})} - 1}\right]\right) \tag{26}$$

For the upper surface, $P_o = 1$ and $k = 0.35M_\infty^{2.29}\sqrt{\lambda}$; on the lower surface, $P_o = 1.55M^2\theta^2$ and $k = 0.12M_\infty^{2.29}\sqrt{\lambda}$. Observe that the upper surface has greater wetted area than the lower one because of the chosen prismatic configuration; while the lower surface area is approximately $A_{\text{lower}} = \ell^2\mathcal{R}/4$, the upper surface area is, following the model of Fig. 6, $A_{\text{upper}} = \ell^2\sqrt{\tan^2\theta + \mathcal{R}^2/16}$. The overall drag coefficient is then the sum of the integral of streamline C_D over both surfaces.

For the special case of small Knudsen number,

$$D_{\text{visc}} = (0.45\sqrt{\mu})M_\infty^{n-1}\sqrt{\rho}U^{3/2}\ell^{3/2}\left(\frac{\gamma - 1}{2}\right)^{\frac{1}{2}(n-1)} \times \left\{0.62\mathcal{R}\, M_\infty\theta + \sqrt{\frac{\mathcal{R}^2}{16} + \tan^2\theta}\right\} \tag{27}$$

In a CO_2 atmosphere,

$$D_{visc} = (0.54\sqrt{\mu})M_\infty^{-0.21}\sqrt{\rho}U^{3/2}\ell^{3/2}\left\{0.62\mathcal{R}\,M_\infty\theta + \sqrt{\frac{\mathcal{R}^2}{16} + \tan^2\theta}\right\} \quad (28)$$

Designing for Maximum Lift/Drag

Using the preceding results for lift and overall drag, several design trends will lead to maximize L/D:

1) Overall length ℓ should be as large as possible.

2) When significant leading-edge bluntness is present, aspect ratio should be decreased (i.e., wider waveriders are undesirable).

3) In the absence of leading-edge bluntness, aspect ratio has little effect on L/D for a given overall length.

4) Altitude should be as low as possible.

Table 1 presents maximum L/D values for the Venus cruise portion of the Earth-Venus-Mars-Sun trajectory as a function of vehicle length. All waveriders are designed for 80-km altitude in the Venus atmosphere. Note that the larger the vehicle, the higher the value of L/D that can be obtained because viscous drag is reduced relative to other forces. Also shown is the effective incident angle θ associated with maximum L/D. Smaller vehicles tend toward larger θ because wave drag must offset viscous effects. These simple analytical results match computational results extremely well. Figure 7 summarizes maximum L/D across a wide range of vehicle lengths.

Generally, leading-edge bluntess will have a negligible effect on L/D as typical values of $\bar{R}_{LE}$ will be on the order of 10^{-2}–10^{-4}. Figure 8 presents L/D for a 10- and a 50-m-long waverider at 80-km altitude in the Venus atmosphere. Note that for the expected range of bluntness, leading-edge effects are barely noticeable. This is particularly reassuring if leading-edge ablation is to be expected.

The analytical model predicts that L/D performance is nearly independent of aspect ratio. This has been confirmed by detailed computational codes, which have occasionally produced multiple optimized waveriders for certain flight conditions which vary dramatically in width for a given length but have nearly identical L/D. This also implies that ablation will have negligible effect on the waverider performance unless leading-edge bluntness is so severe that the pressure containment provided by the leading-edge bow-shock attachment is lost.

Calculations of the L/D ratio suggest that the fractional decrease in L/D associated with lift reduction during the flight is greater at higher values of L/D. Examples will be presented below. This result is understandable since high L/D typically translates into very small drag, so any change in vehicle performance that produces noticeably more drag will have a strong effect on L/D. It is further apparent that the waverider aerodynamic performance will be more constant through an aerogravity assist if 1) the waverider is as long and wide as possible; 2) flight is at the lowest possible altitude; and 3) velocities are as high as possible, since required lift scales approximately with the square of flight velocity.

Unfortunately, the trend to flight at lower altitudes will also increase the heating problems on the vehicle. Temperature estimates will be presented below for sample waverider flights. Radiative equilibrium was assumed at the stagnation point with emissivity of 0.8, balanced by the energy released in the dissociation of CO_2, 382 kcal/g-mole.

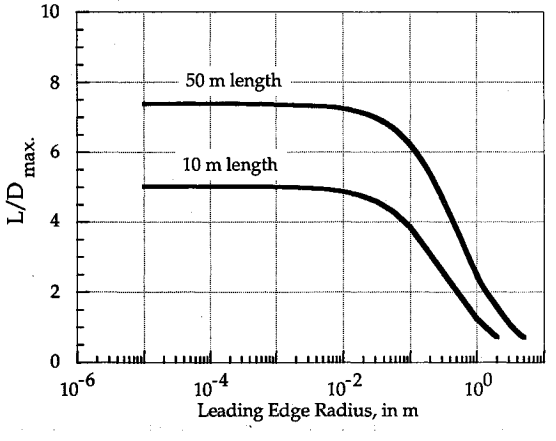

Fig. 8 Variation in maximum L/D with leading-edge bluntness, for flight at 80 km in the Cytherean atmosphere. Two lengths are considered, 10 and 50 m.

Sample Atmospheric Flight

In the Earth-Venus-Mars-Sun mission, the preceding concepts can be demonstrated for a sample waverider vehicle. Consider a satellite with mass 5000 kg on a waverider that is 10 m long and 2 m wide.

With an approach velocity of 17.470 km/s, the spacecraft will enter the Venus atmosphere at 20.25 km/s, at about Mach 80 (compared to Mach 65 for Galileo's Jovian entry), at 80-km altitude. With a 20-cm leading edge, stagnation temperatures will reach 10,000 K; 14,000 K with a 10-cm radius, neglecting ionization effects. The spacecraft flies through approximately 62 deg for 5 min 34 s; with constant $L/D = 7$, the spacecraft loses 2.53 km/s to drag; with a more likely $L/D = 5$, the loss is 3.37 km/s. Although the initial velocity could be increased to compensate for this loss, it is best made up with an engine firing at the end of the maneuver, as shown in Ref. 15.

Acceleration will be 5.75 terrestrial g at the start of the maneuver, dropping down to 4.2 g at atmospheric exit. These values are higher than those typically specified for sustained human flight (3 g), but within the range commonly experienced by pilots.

The preceding modeling estimates that, with an initial $L/D = 7$, it will emerge with final $L/D = 5.8$; and with initial $L/D = 5$, the final $L/D = 4.8$. Higher L/D vehicles will suffer a noticeable loss in performance, reducing their overall advantages vs lower L/D shapes. At exit stagnation heating will have abated, so the 10-cm-radius leading edge will have equilibrium temperature of 13,500 K, and the 20-cm radius will be at 8350 K. The waverider leaves Venus at 14.459 km/s relative speed if initial $L/D = 7$, having lost 3.011 km/s to drag losses; with initial $L/D = 5$, the loss is 4.05 km/s. The total ΔV of the maneuver is 21.64 km/s at $L/D = 7$.

Conclusions

The use of aerodynamic lifting force for the manipulation of spacecraft trajectories depends ultimately on the feasibility of designing hypersonic configurations with L/D values of approximately 7–10 and retaining that performance for the duration of the flight. Regardless of the details of the particular atmospheric trajectory chosen, higher L/D always translates into a more effective aeroassisted flight because it enables larger angular deflections for a given energy loss.

This work has used simple modeling to address some basic performance questions. For the trajectories featured here, acceleration levels and heating rates are beyond the limit of current technology. Although unmanned spacecraft may be capable of 6 g sustained flight, 14,000 K leading-edge temperatures for 5-min intervals go beyond even the extremes of temperatures predicted for the Galileo atmosphere probe (11,000 K). However, they are not so large that it is impossible to envision future technology capable of accepting such a thermal environment.

Aerodynamic performance will certainly suffer during an aeroassisted flight. In the example presented, a drop in L/D from 7 to 5.3 is not particularly dramatic, but it does translate directly into losses that must be compensated for with on-

board propulsion. This also suggests that the advantages of high L/D are not as great as the constant L/D predicts. Also, the dependence of L/D on viscous effects and the strong influence of ambient density through the Reynolds number casts doubt on the viability of using one waverider shape for more than one aeropass at different flight conditions.

If they are viable, some general design rules should be adhered to in designing planetary waveriders. The dimensional arguments suggest that, for maximum aerodynamic efficiency, they should be as long as possible, although width has little impact on performance. Additionally, low-altitude flight, which results from high required wing loading, provides better performance, albeit at the cost of higher heating rates.

This work suggests that more concern should be devoted to the off-design characteristics of waveriders, not only for changes in Mach number and angle of attack but changes in ambient density as well. A study of the effect of leading-edge bluntness on the leading-edge attachment is sorely lacking. In addition, more detailed studies of heating patterns and an address of control issues will be paramount if the aerogravity-assisted flight concept is to be made a viable option for space mission planners.

Acknowledgments

The authors gratefully acknowledge the assistance of John D. Anderson Jr. of the Department of Aerospace Engineering at the University of Maryland, and James Randolph of the Jet Propulsion Laboratory in preparing this document and discussing many of the ideas contained within. David Bender and Stacy S. Weinstein, also of the Jet Propulsion Laboratory, supplied much information on the aeroassisted trajectory analysis. A portion of this work was supported by a grant from NASA and the University Space Research Association, to whom appreciation is also expressed. Additional computer support has been provided by the Jet Propulsion Laboratory.

References

[1]Walberg, G. D., "A Survey of Aero-Assisted Orbital Transfer," *Journal of Spacecraft and Rockets,* Vol. 22, No. 1, 1985, pp. 3–18.

[2]Wilhite, A. W., Arrington, J. P., and McCandless, R. S., "Performance Aerodynamics of Aero-Assisted Orbital Transfer Vehicles," AIAA Paper 84-0406, Jan. 1984.

[3]Bletsos, N. A., "Performance and Control with Lift Modulation of Hypervelocity Entry Vehicles," Ph.D. Thesis, Univ. of Michigan, Ann Arbor, MI, 1976.

[4]Randolph, J. E., and McRonald, A. D., "Solar Probe Mission Status," American Astronomical Society Paper 89-212, Greenbelt, MD, April 1989.

[5]Lewis, M. J., "The Use of Hypersonic Waveriders for Aero-Assisted Orbital Maneuvering," *Proceedings of the 30th International Conference on Aviation and Space,* Univ. of Tel Aviv, Tel Aviv, Israel, Feb. 1990.

[6]Lewis, M. J., and Kothari, A. P.,"The Use of Hypersonic Waveriders for Planetary Exploration," 2nd International Conf. on Solar System Exploration, Aug. 1989.

[7]Nonweiler, T. R. F., "Aerodynamic Problems of Manned Space Vehicles," *Journal of the Royal Aeronautical Society,* Vol. 63, 1959, pp. 521–528.

[8]Corda, S., and Anderson, J. D., "Viscous Optimized Hypersonic Waveriders Designed from Axisymmetric Flow Fields," AIAA Paper 88-0369, 1988.

[9]Bowcutt, K. G., Anderson, J. D., and Capriotti, D., "Numerical Optimization of Conical Flow Waveriders Including Detailed Viscous Effects," *Aerodynamics of Hypersonic Lifting Vehicles,* AGARD Conf. Proceedings No. 428, Nov. 1987, pp. 27-1–27-23.

[10]Bowcutt, K. G., Anderson, J. D., and Capriotti, D., "Viscous Optimized Hypersonic Waveriders," AIAA Paper 87-0272, 1987.

[11]Anderson, J. D., Lewis, M. J., Kothari, A. P., and Corda, S., "The Design of Hypersonic Waveriders for Entry into Foreign Planetary Bodies," AIAA Paper 90-0538, Jan. 1990.

[12]McLaughlin, T. A., "Viscous Optimized Hypersonic Waveriders for Chemical Equilibrium Flow," M.S. Thesis, Dept. of Aerospace Engineering, Univ. of Maryland, College Park, MD, June 1990.

[13]Anderson, J. D., Jr., "A Survey of Modern Research in Hypersonic Aerodynamics," AIAA Paper 84-1578, 1984.

[14]White, F. M., *Viscous Fluid Flow,* McGraw-Hill, New York, 1974, pp. 620–623.

[15]Lewis, M. J., and Kothari, A. P., "Space Propulsion Benefits With High L/D Aero-Assisted Maneuvering," AIAA Paper 90-2368, July 1990.

Ernest V. Zoby
Associate Editor